Journal of Archaeological Science 135 (2021) 105477

Contents lists available at ScienceDirect

Journal of Archaeological Science

journal homepage: www.elsevier.com/locate/jas

Diagenesis of juvenile skeletal remains: A multimodal and multiscale approach to examine the post-mortem decay of children's bones

Valentina Caruso, PhD, researcher [a,f,*], Nicoletta Marinoni, Associate professor [a], Valeria Diella, PhD, Researcher [b], Elena Possenti, PhD, researcher [c], Lucia Mancini, PhD, senior beamline scientist [d], Marco Cantaluppi, PhD student, PhD student [a], Francesco Berna, Associate professor, Associate professor [e], Cristina Cattaneo, Professor, Professor [f], Alessandro Pavese, Professor, Professor [g]

[a] *Dipartimento di Scienze della Terra "Ardito Desio", Università degli Studi di Milano, Luigi Mangiagalli street n. 34, 20133, Milan, Italy*
[b] *Consiglio Nazionale delle Ricerche, IGAG, Sezione di Milano, Sandro Botticelli street n. 23, 20133, Milano, Italy*
[c] *Consiglio Nazionale delle Ricerche, ISPC, Sezione di Milano, Roberto Cozzi street n. 53, 20125, Milano, Italy*
[d] *Elettra-Sincrotrone Trieste S.C.p.A, S.S. 14 - km 163,5, 34149, Basovizza, Trieste, Italy*
[e] *Department of Archaeology, Simon Fraser University, 8888 University Drive, Burnaby, British Columbia, Canada*
[f] *LABANOF, Laboratorio di Antropologia e Odontologia Forense, Sezione di Medicina Legale e delle Assicurazioni, Dipartimento di Scienze Biomediche per la Salute, Università degli Studi di Milano, Luigi Mangiagalli Street n. 37, 20133, Milan, Italy*
[g] *Dipartimento di Scienze della Terra, Università degli Studi di Torino, Valperga Caluso street n. 35, 10123, Turin, Italy*

ARTICLE INFO

Keywords:
Juvenile bone diagenesis
Virtual histology
Synchrotron X-ray computed microtomography
X-ray powder diffraction
Fourier transform infrared spectroscopy
Electron microprobe analysis

ABSTRACT

This study aimed to examine the degradation of juvenile skeletal remains with respect to adult counterparts from different burial settings in Milan, Italy. A multiscale and multimodal approach was applied to investigate bone diagenesis by combining chemical and mineralogical analyses with synchrotron radiation-based virtual histology. Certain differences could be observed between child and adult skeletal remains; juvenile bones exhibited (*i*) poorer histological conservation, with prominent general re-organisation of the observed three-dimensional original microstructure, resulting in denser structures with low porosity; (*ii*) bioapatites with low defective structures, with chemical compositions highly site-sensitive, exhibiting variation even within a single bone; (*iii*) organic matter highly variable in terms of quality, quantity, and arrangement, even within a single bone sample. Conversely, organic decay results in similar enrichment in calcium content both in juveniles and in adults. In conclusion, the present work points out high intra-individual skeletal preservation in archaeological juvenile bones with respect to adults, thus suggesting that immature and mature bone tissues deteriorate at different rates, foremost as a function of their intrinsic features (shape, porosity, histological structures, etc.), and secondarily under the influence of the burial environment.

1. Introduction

In bioarchaeology and forensic anthropology, accurate characterisation of the biological and pathological profile of retrieved juvenile skeletal remains is critical (Booth et al., 2016).

The mortality rate of infants (0–3 years) and children (or juveniles, 4–14 years) in past cultures was over 40% due to abortion, infanticide, environment, physical stress, disasters, and lifestyle (Ērkšķe, 2020).

It is estimated that only about 11% of child graves in archaeological cemeteries in Europe were retrieved until the first decade of the twenty-first century (Chacheva, 2015). Therefore, bioarchaeological evidence of subadults (i.e. those under 18 years old) was seriously under-represented in pre-industrial societies. Furthermore, the hypothesis that children's bones decompose more rapidly than adults' due to their smaller size, incomplete mineralisation, higher organic content, and greater porosity seems to be well confirmed (Buckberry, 2000;

* Corresponding author. Dipartimento di Scienze della Terra "Ardito Desio", Università degli Studi di Milano, Luigi Mangiagalli street n. 34, 20133, Milan, Italy.
E-mail addresses: caruso.valentina@libero.it (V. Caruso), nicoletta.marinoni@unimi.it (N. Marinoni), valeria.diella55@gmail.com (V. Diella), possenti@icvbc.cnr.it (E. Possenti), lucia.mancini@elettra.eu (L. Mancini), marco.cantaluppi@unimi.it (M. Cantaluppi), francesco_berna@sfu.ca (F. Berna), cristina.cattaneo@unimi.it (C. Cattaneo), alessandro.pavese@unito.it (A. Pavese).

https://doi.org/10.1016/j.jas.2021.105477
Received 19 April 2021; Received in revised form 31 August 2021; Accepted 1 September 2021
Available online 9 September 2021

Djurić et al., 2011; Lewis, 2007; Manifold, 2010, 2012, 2013).

In the last few years, rescue excavations increased the total available bioarchaeological data collected from juvenile human skeletal remains to over 50% (Borić and Stefanović, 2004; Caruso et al., 2013; Cattaneo et al., 2015; Chacheva, 2015; Ērkšķe, 2020; Gardeła and Duma, 2013; Georgiadis, 2011; Groza et al., 2020; Kay, 2016; Stroszeck, 2012 and references therein). Ethnographic and anthropological data show that in several ancient communities, the mortuary rituals for infants and children differed from those for adults, owing to factors such as different civic values, incomplete development of the soul, lack of emotional attachment, or on the other side also extreme reverence (Ērkšķe, 2020). For instance, in the Neolithic period, infants were interred in shallow graves and buried under domestic spaces, outside their dwellings, or in public areas, and were considered 'protective spirits' (Ērkšķe, 2020; Georgiadis, 2011). In Ancient Greece and the Early Roman period, foetuses and infants were buried inside urns, amphorae, and domestic pots, to reproduce the effect of the maternal womb (Chacheva, 2015; Stroszeck, 2012). Furthermore, children and adolescents were commonly buried in the same grave-pits as adults, either in multiple inhumations organised by familial groupings or in single or multiple tombs located in specific areas of the cemetery.

Apart from burial conditions, the survival of a bone is influenced by its intrinsic features. A human bone is a hierarchically composite biomaterial, with mineralised collagen fibrils as its basal building component (Weiner and Wagner, 1998). A juvenile bone's components are 66 wt% of mineral nanoparticles (carbonated hydroxyapatite, CHA), 20 wt% of proteins (mainly type I collagen), and 14 wt% of water (Guy et al., 1997). The organo-mineral fraction of *in vivo* bone, in terms of quality, quantity, and microstructure, reflects a combination of multiple factors – including sex, age, diet, ethnicity, metabolisms, diseases, and treatments – which affect the biomechanical properties of bones (Barth et al., 2011; Fratzl et al., 2004; Manifold, 2014).

The close association between collagen and minerals elucidates the processes involved in bone diagenesis (Keenan, 2016). The perimortem amount of the organic and mineral components – as well as their three-dimensional (3D) spatial organisation – considerably affects the post-mortem preservation of bones. After death, bone decay is unpredictable as the human body interacts with its burial environment (Caruso et al., 2018; Keenan and Engel, 2017; Kontopoulos et al., 2016, 2019).

Bone tissue decay of adult humans is primarily characterised through either macro- or micro-scopic bone morphology (Caruso et al., 2018; Jans et al., 2002, 2004; Turner-Walker et al., 2002), or physicochemical bone properties (Bayari et al., 2020; Beasley et al., 2014; France et al., 2014; Hollund et al., 2013; López-Costas et al., 2016; Piga et al., 2009), or porosity (Nielsen-Marsh and Hedges, 2000; Smith et al., 2008; Turner-Walker, 2019). However these aspects are rarely taken into account in conjunction (Caruso et al., 2020; Dal Sasso et al., 2014, 2016; Kontopoulos et al., 2019; Smith et al., 2002; Turner-Walker and Syversen, 2002).

Few studies have investigated the diagenesis of child bones in archaeological contexts focusing on (*i*) the macroscopic bone appearance (Manifold, 2010, 2013); (*ii*) the degree of bone mineralisation (Manifold, 2014); (*iii*) the bone microbial bioerosion (White and Booth, 2014; Booth, 2016; Booth et al., 2016; Goren et al., 2020); (*iv*) the histo-morphometry of osteons and vascular system (Pitfield et al., 2019); and (*v*) the preservation of the organo-mineral bone fraction (Bayari et al., 2020).

Nevertheless, significant research is required to better understand bone degradation in burial, due to the complexity and unpredictability of post-mortem changes (Smith et al., 2002). This is a preliminary work that aims to garner insights into the various processes (i.e. microbial bioerosion, chemical elements uptaken, mineral changes, and degradation of collagen protein) that affect the decay of juvenile skeletal remains, to contribute to the completeness of their archaeological and forensic record with a multimodal and multiscale approach.

Eight cortical long bones were selected from different juvenile skeletons buried in three necropolises of Northern Italy, spanning from the Late Roman age (3rd century AD) to the Modern age (17th century AD).

The mineral fractions of the cortical bone tissue for each sample were investigated using mineralogical, spectroscopic, and chemical methods (high-resolution X-ray powder diffraction [XRPD], electron microprobe analysis [EMPA], and Fourier transform infrared [FT-IR]). The internal cortical bone microstructure was explored with conventional two-dimensional (2D) histological observations and three-dimensional (3D) analyses from phase-contrast synchrotron radiation computed microtomography (Hesse et al., 2014; Nava et al., 2017; Pacureanu et al., 2014; Sanchez et al., 2012; Smith et al., 2010). In particular, the high resolution of the synchrotron virtual histology enabled the rendering of the bones' 3D internal architecture, which included the spatial organisation and integrity of the cortical bone porosity (Caruso et al., 2020).

The organo-mineral preservation, chemical substitution, and 3D porosity measurement of the juvenile bones were compared with that of adult skeletons having the same archaeological ages and burial proveniences (Milan area; Caruso et al., 2020).[1]

2. Materials

2.1. Bone sampling

Eight long bones (femur, tibia, and humerus) were chosen from juvenile skeletons recovered from three different archaeological sites in Northern Italy. As reported in Supplementary Table S1, two skeletons were sampled from a Roman necropolis discovered at the 'Università Cattolica' of Milan (3rd–4th century AD – Late Roman age); two skeletons belonged to the necropolis discovered in 'Via Monte Napoleone' in Milan (15th–16th century AD – Middle age); two skeletons come from a mass grave discovered in 'Viale Sabotino' in Milan (17th century AD–Modern age). The percentage of subadults recovered and studied in the last years was ~40% on a total of 633 recovered individuals (work unpublished) from the first necropolis of ~30% of 102 individuals (work unpublished), and ~23% of 240 individuals in the second and third one, respectively (Caruso et al., 2013).

The age at death was calculated by analysing the tooth development (Ubelaker, 1978) and epiphyseal union stage and diaphyseal length of long bones (Scheuer and Black, 2000). Due to skeletal immaturity, diagnosis of sex was not performed.

From each long bone, four adjacent cross-sections of cortical mid-diaphysis were taken using a diamond-coated rotary saw, and each section was employed for our 2D histological analysis, synchrotron radiation microtomography, EMPA, FT-IR, and XRPD analyses.

3. Methods

3.1. Histological analysis

Thin cross-sections were prepared following Caruso et al. (2018) and analysed by optical microscopy using an Axio Scope A1, equipped with a True Chrome HD II camera at a resolution of 1920 × 1080. Bone images were acquired using the software IScapture® (version 3.6.7).

Histological assessment of each bone was quantified using the

[1] Adult and juvenile bones dated back to the Late Roman and Modern age and came from the same archaeological burial sites of Milan, specifically from the necropolis of Università Cattolica and the mass grave of Viale Sabotino; whereas adult and juvenile Middle age bones were collected from two different archaeological sites of Milan, specifically the cemetery of Ca' Granda and the necropolis of Via Monte Napoleone, respectively, both located within an area of less than 1 km radius.

Oxford Histological Index (OHI; Hedges et al., 1995) as reported in Supplementary Appendix A1.

3.2. Synchrotron radiation microtomography (SR-μCT)

Synchrotron radiation propagation-based phase-contrast SR-μCT was used to obtain the 3D virtual reconstruction of the microstructure of examined bone volumes. Parallelepiped-shaped bone samples (10 mm × 5 mm x 2 mm) were imaged at the SYRMEP (SYnchrotron Radiation for MEdical Physics) beamline of the Elettra synchrotron laboratory (Basovizza [Trieste], Italy), employing a filtered (1 mm Al + 1.5 mm Si) polychromatic X-ray beam delivered by a bending magnet source in transmission geometry. The detector used was a water-cooled, 16-bit, scientific Complementary metal–oxide–semiconductor (sCMOS) macroscope camera (Hamamatsu C11440–22C) with a 2048 × 2048 pixels chip coupled with an LSO:Tb scintillator screen (17 μm-thick on the top of a 170 μm-thick LSO substrate) through a high numerical aperture optics. The effective pixel size of the detector was set at 0.9 × 0.9 μm^2, yielding a maximum field of view of about 1.8 × 1.8 mm^2. The sample-to-detector (propagation) distance was set at 150 mm. A set of 1200 projections were recorded, with continuous sample rotation over a 180-degree scan angle and an exposure time per projection of 2.5 s.

Each set of acquired raw images was processed using the SYRMEP Tomo Project (STP) software suite, developed in-house at Elettra (Brun et al., 2015) based on the ASTRA Toolbox (Van Aarle et al., 2015), to perform the CT reconstruction employing the Filtered Back-Propagation algorithm using a filter (Rivers, 1998) to reduce the so-called ring artefacts in the reconstructed slices. A single-distance phase retrieval algorithm was applied to projection images before CT reconstruction (Paganin et al., 2002), setting a γ parameter (ratio between the real and imaginary parts of the complex refraction index of the material under investigation) of 30. First, bone porosity was measured from the bone volume, and the osteocyte lacunae, vascular canal networks, and pores produced by diagenesis were recognised and differentiated. Second, the pore distribution of the vascular canal pores (size, volume fraction, connectivity, morphometric features) within the imaged sample volume was obtained. The data processing used to provide image segmentation and histomorphometric analyses were performed per Caruso et al. (2020), as reported in detail in Supplementary Appendix A2.

3.3. Electron microprobe analysis (EMPA)

EMP-WDS was employed to carry out backscattered electron images and quantitative chemical analyses on thin sections, using a JEOL JXA-8200 EMP-WDS, with an accelerating voltage of 15 kV, a beam current of 5 nA, and counting times of 30 s, on the peak, and 10 s, on the background. Quantitative analysis of major (Ca, P) and minor (Fe, Al, Na, K, Si, Mn, Mg, Sr, Ba, S, Cl) elements was performed and natural minerals were used as standards. Raw data were corrected for matrix effects using a conventional ΦρZ routine in the JEOL software package.

3.4. Fourier transform infrared (FT-IR) spectroscopy

For FT-IR spectroscopy, the samples were prepared in KBr pellets following Trueman et al. (2008). Bone powders were analysed in transmission mode using a Thermo Scientific™ Nicolet™ iS50 FT-IR Spectrometer equipped with a DTGS detector (spectral range 4000–400 cm^{-1}). The absorption spectra were collected with a spectral resolution of 2 cm^{-1} and by recording 64 scans. The reproducibility of the observations was assessed by duplicate measurement of each sample. Instrumental operations, spectra collections, and data analyses were carried out using the Thermo-Nicolet Omnic (version 9) software. In particular, for each bone sample, the vibrational features and absorbance of Amide I (1653 cm^{-1}), $\nu_3(PO_4)$ (1035 cm^{-1}), and $\nu_2(CO_3)$ (873 cm^{-1}) were studied, following Caruso et al., (2020), as reported in Supplementary Appendix A3.

3.5. X-ray powder diffraction (XRPD)

Bone samples for bulk XRPD were pulverised and back-loaded on a flat Al sample-holder and measured using a Bragg-Brentano geometry PANalytical X'Pert Diffractometer, using CuKα radiation (1.5417 Å) operating at 40 kV and 40 mA, with an X'Celerator detector. Data were collected over an angular range (2θ) of 5°–140° with a divergence slit of 1/4° and a receiving slit of 0.1 mm as instrumental set-up. The XRPD patterns were collected with a counting time of 100 s/step and with a 0.01° step, and the collection time for each powder pattern was applied for 120 min. In accordance with Caruso et al. (2020), XRPD qualitative analysis was performed using PANalytical X'Pert HighScore software. Rietveld refinement (Young, 1993) was performed on diffraction patterns using the GSAS-II program as reported in Supplementary Appendix A4.

4. Results

4.1. Histological analysis

As illustrated in Fig. 1, the bone histology of analysed bones appeared generally poorly preserved, massively eroded by microbes (*sensu stricto* bacteria and fungi), and does not preserve any original microstructural features, except for Haversian canals. As reported in Supplementary Table S2, about 80% of bones showed a low OHI value (0–1; Fig. 1a and c), except for one Middle age sample (*VM_1J,* OHI = 3). In the latter, the original microstructure appeared undamaged where secondary osteons and interstitial lamellae can be easily recognised, even though some foci of destruction due to the microbial activity appeared to be present around Haversian canals (Fig. 1b).

4.2. Synchrotron X-ray microtomographic analysis

An example of the image analysis on a volume of cortical bone tissue under the periosteal border is provided in Fig. 2. The 3D original bone porosity (osteocyte lacunae [Hesse et al., 2014] and Haversian canals) was rendered (Fig. 2e) and measured starting from the data segmentation (Fig. 2d) of 2D virtual slices (Fig. 2a, b, and c). Similarly, the diagenetic pores were analysed; they appeared irregular in terms of morphology and size, frequently interconnected and breaking the osteon network.

The analysis of total volume renderings performed (an example is illustrated in Supplementary Fig. S1Supplementary Fig. S1) found modest different degrees of preservation of natural and diagenetic pores in terms of the vascular canal's shape, diameter, volume, and interconnections.

The quantitative analysis (Fig. 3a) indicated that the Middle age sample (*VM_1J*) exhibited the highest percentage of TP concerning bones of the Late Roman age (*UC_2J*) and the Modern age (*VS_1J*). In all bones, a small part of the percentage of TP derived from diagenetic porosity (DP). The percentage of CP, concerning TP, remained high in all the samples (86–66%), even if a positive correlation with the archaeological age was not observed, as the most ancient bone (*UC_2J*) had the highest percentage of CP compared to the most recent bones (*VM_1J* and *VS_1J*). At the same time, the lowest value of DP (~14%) was detected in the Late Roman age sample (*UC_2J*), in comparison to the other bones (*VM_1J* and *VS_1J*).

The morphometric analysis of vascular canal volume provided a high percentage of meso- (10^{-8} < volume >10^{-6}) and macro-pores (volume >10^{-5} mm^3), as plotted in Fig. 3c.

The vascular canal diameters appeared quite different among samples, in particular, the bone of the Late Roman age (*UC_2J*) had the lowest average value (0.016 mm), similar to the value of the bone of the Modern age (*VS_1J,* 0.022 mm), whereas in the bone of the Middle age (*VM_1J*), the average value was higher (0.039 mm). In all samples, the vascular canal connection seemed almost negligible.

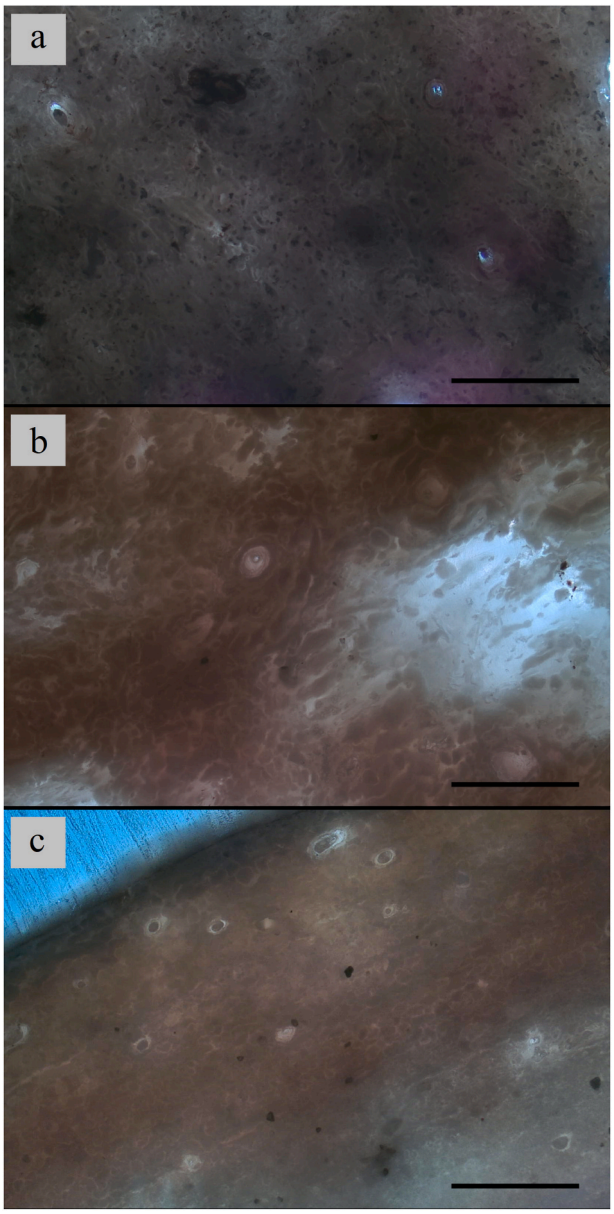

Fig. 1. Histological analysis of optical microscopy performed on juvenile bones. An example of typical microscopical degradation is displayed for each archaeological age. a) *UC_2J* sample of the Late Roman age with an Oxford Histological Index (OHI) = 0; b) *VM_1J* sample of the Middle age with an OHI = 3; c) *VS_1J* sample of the Modern age with an OHI = 0 (scale bar: 250 μm).

4.3. Electron microprobe analysis (EMPA)

The BSE images of the cortical bone tissues highlighted a widespread alteration of original bone microstructures from periosteal to endosteal borders. In particular, in each image three different regions could be observed according to the greyscale values (Fig. 4).

In samples of the Late Roman (*UC_2J*) and Modern age (*VS_1J*; Fig. 4a and c) *altered zones* were widespread within the tissue. These were irregular, black, and contained numerous voids, and were generally surrounded by micrometric rings of *re-mineralised zones* because of microbial damage.

Only in the sample of the Middle age (*VM_1J*), the tissue appeared well preserved and *altered* and *re-mineralised zones* were restricted to the Haversian canals, with large, regular, and circular voids (Fig. 4b).

In all samples, the carbonated hydroxyapatite (CHA) represented the only preserved mineral phase within the bone, and its crystal samples shared a similar average chemical composition in terms of major oxides.

Point chemical analyses – performed in the three identified microstructural zones from the periosteal to the endosteal border of the cortical bone tissue – highlighted significant differences in terms of composition (Table 1). As illustrated in Supplementary Fig. S2Supplementary Fig. S2, all bones comprised high CaO wt% and P_2O_5 wt% contents in *unaltered* and *re-mineralised zones* (45–50 wt% and 31–35 wt%, respectively). In the *altered zones* the CaO and P_2O_5 exhibited, as expected, a wide range of variation.

The high value of the sum of the total oxide contents (~80 wt%) was detected in all bones and may be ascribed to the low contents of organic carbon (approximately 7 wt% in *in vivo* bone, from Wopenka and Pasteris, 2005), lipids, and water within the CHA structure.

Considering the minor elements (i.e. with concentrations <1 wt% in oxide), a high ionic substitution in the mineral structure of Ca^{2+} and P^{3+} was detected in all samples, as presented in Supplementary Fig. S3Supplementary Fig. S3. In bone CHA, calcium and phosphorous can be replaced by several chemical complexes (Keenan et al., 2015; Krajcarz, 2019; Margariti et al., 2019; Nielsen-Marsh et al., 2000; Rogoz et al., 2012; Wopenka and Pasteris, 2005 and references therein). In this study, Na^+ and Mg^{2+} occurred in all samples, whereas Fe^{2+} occurred only in *UC_1J* and *VS_1J* bones. Substitution of $SO_4^{2-}$and in a lower amount of SiO_4^{4-}, in place of PO_4^{3-}, was observed in all samples with a high level of SO_3 detected in *unaltered zones* of all bones and that of SiO_2 in those of *VS_1J* bones.

As to the ionic substitution of the OH^- group, F^- results below the detection limit, and Cl^- was similar in all bones examined.

4.4. Fourier transform infrared (FT-IR) spectroscopy

The FT-IR spectra of Fig. 5 showed a low absorbance at Amide I and $\nu_2(CO_3)$ bands in all bones. As reported in Supplementary Table S3, the bones of the Late Roman and Modern age shared the same value of Amide I to phosphate ratios (0.11), which slightly increased in the samples of the Middle age (0.18). Hence, the estimated fraction of organic matter grew from ~22.5 wt% to ~24 wt% in these bones. The carbonate to phosphate ratio was the same in all specimens (0.08 in mean).

On the contrary, the calculated IRSF increased with the age of samples (up to 3.5 in the samples of the Late Roman age). Based on the IRSF, the calculated mean crystal length of bone minerals changed from ~41 to ~56 nm with aging. Therefore, an inverse correlation can be established between the IRSF and Amide I content, and the same holds between the carbonate content and IRSF values.

4.5. X-ray powder diffraction (XRPD)

The XRPD results highlighted that all specimens were mainly composed of hydroxyapatite; both bones of the Late Roman age and one bone of the Modern age (*VS_1J*) had discrete amounts of quartz (10–30%).

Both isotropic and anisotropic models were used to perform profile fitting. However, the uniaxial model gave significantly better results, because it is more appropriate to describe the crystallites shape (Caruso et al., 2020).

Through a close inspection of the diffraction profiles reported in Fig. 6, the XRPD line broadening of the [001] peak of hydroxyapatite was less narrow in all samples, revealing lower crystallinity of the crystallites. In general, XRPD patterns of hydroxyapatite highlighted a very small average crystallite size, whose shape was elongated along the *c*-axis (Supplementary Fig. S4(a)Supplementary Fig. S4a); *c*-axis crystallite size significantly decreased with the antiquity of the sample (240 Å; Supplementary Fig. S4(b)Supplementary Fig. S4b). The equatorial component of the uniaxial model was similarly low (140 Å). Cell parameters refinement on hydroxyapatite revealed little cell volume changes among samples, ranging from 530 to 532 $Å^3$, which falls within

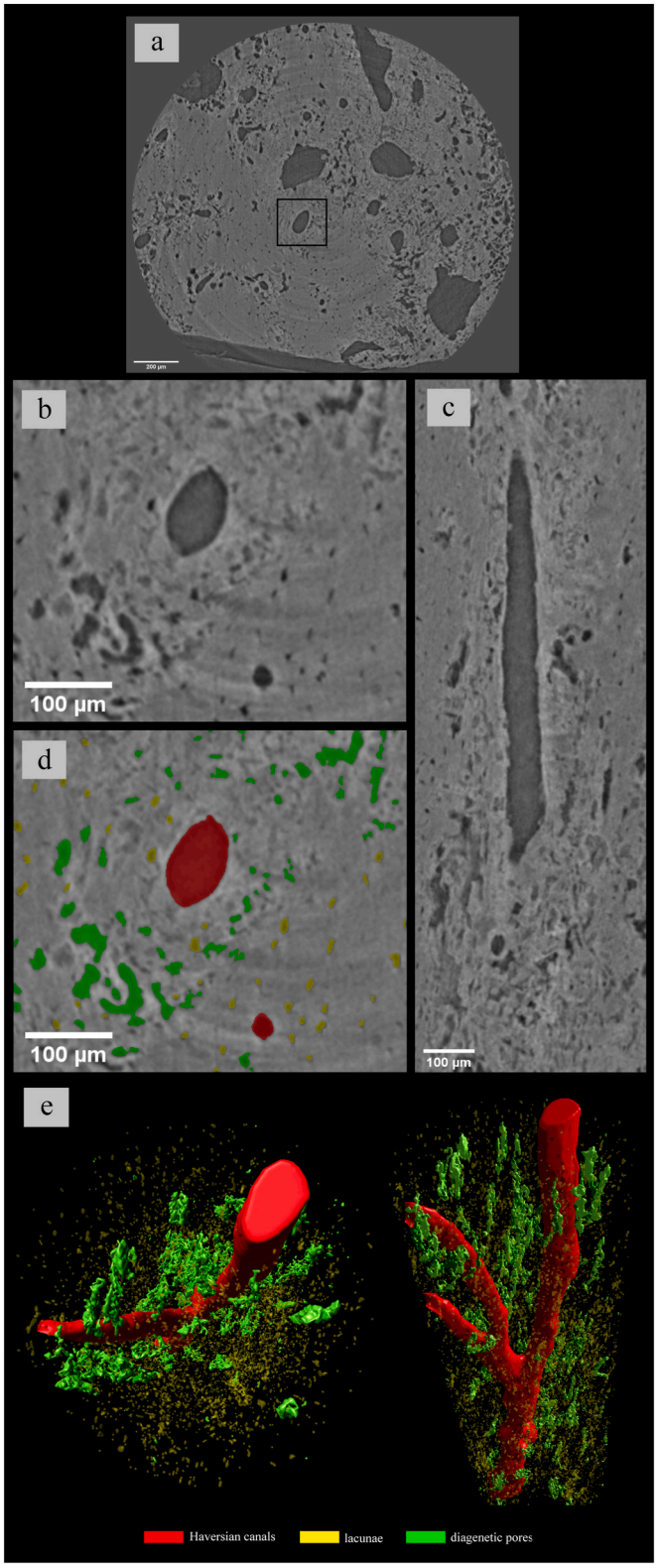

(caption on next column)

Fig. 2. a) two-dimensional (2D) axial slice through the reconstructed three-dimensional (3D) data (voxel size: 0.9 µm); b and c) region of interest of orthogonal slices (xy, yz) selected around an osteon from Fig. 2a (delimited into the black rectangular area). This region was selected to provide a detailed *morphology of a single Haversian canal within the cortical bone section, in relation with the organisation of the osteocyte lacunae network and diagenetic pores*; d) segmentation of the corresponding segmented areas of the bone matrix (background, in black), osteocyte lacunae (in yellow), vascular canals (in red), and diagenetic pores (in green) for the 2D slice presented in Fig. 2a; e) 3D rendering of the osteocyte lacunae network organised around a Haversian canal (left: transverse view; right: frontal view), showing details of the development of one vascular canal (in red) within the bone section and the osteocyte lacunae organisation (yellow) around it. Diagenetic porosity (in green) produced by the tissue damage has been rendered here and appears mainly concentrated near the vascular canals (voxel size: 0.9 µm). (For interpretation of the references to colour in this figure legend, the reader is referred to the Web version of this article.)

the experimental error. A slight increase in the *a*-cell parameter (9.45 Å) was observed in all samples.

While the behaviour of the hydroxyapatite in terms of crystallite size was variable along the *c*-axis, the values of micro-strain was low (0.006–0.08), suggesting that the coherent diffraction domains are large and small defective.

5. Discussion

This study highlights that all cortical juvenile bones exhibit widespread deterioration, owing to progressive microbial bioerosion at a histological scale. This is the most common form of diagenesis occurring in burial (Booth, 2016; Jans et al., 2004; Turner-Walker et al., 2002), developing from periosteal towards endosteal borders. An exception in our study regarding this was a sample of the Middle age (*VM_1J*), whose bioerosion appears chiefly focused around the Haversian canals. As soon as death occurs, fungi and bacteria start producing peculiar diagenetic patterns. These occur in large and irregular grooves, small pores, and interconnected thin channels surrounded by hypermineralised rings. These features result from the recrystallisation of the original bone mineral bioapatite, which proceeds most readily via the canalicular network (Turner-Walker, 2019).

Compared to the histological degradation observed in archaeological adult remains (Caruso et al., 2020), juvenile bones exhibit lower histological conservation, which is almost constant across different sites and over time.

The synchrotron virtual histology shows significant microstructural differences among samples, even within those with the same OHI value. A general poor conservation of the vascular canals in all bones (Bousson et al., 2001; Schnitzler and Mesquita, 2013) is observed, resulting in a full loss of interconnections and high variability in terms of pore morphology. For example, in the sample of the Middle age, large vascular canals were detected, whereas in bones of the Modern and Late Roman age, a general reduction of pore dimensions was observed in terms of volume and diameter. However, the latter specimens differ from each other for the number of vascular canals, leading to a higher vascular canal porosity in Late Roman bones.

Despite the time elapsed after death, reference cortical samples collected from the same bone show large variations of natural porosity due to the inherent heterogeneous structure of the tissue (Smith et al., 2008). In Caruso et al. (2020), the cortical tissue of long adult bones is constituted of 50% Haversian systems and 50% interstitial lamellae, whereas this does not occur in juveniles (Pfeiffer, 2006; Zimmermann et al., 2019).

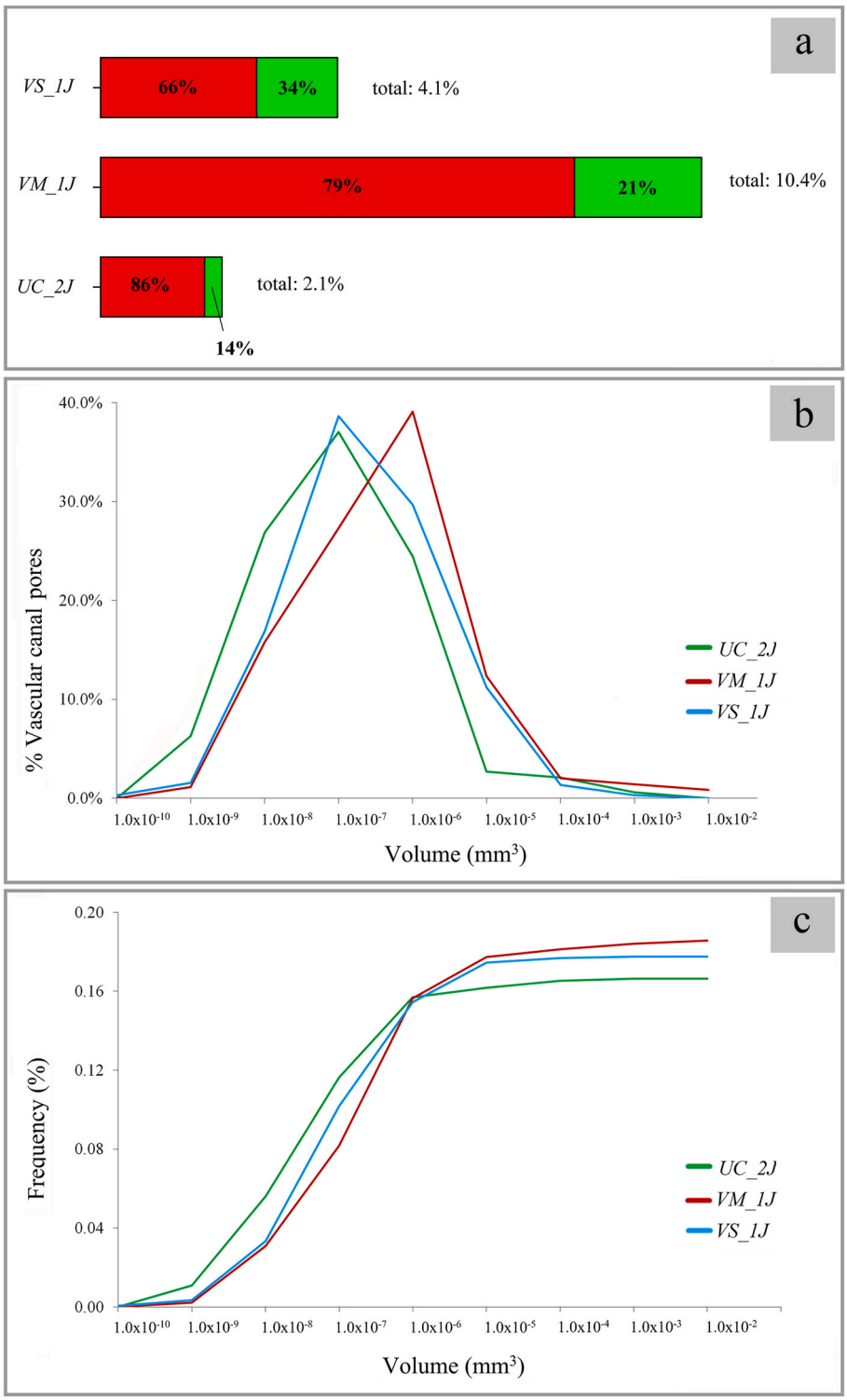

Fig. 3. a) On the scale bars, the percentage of the vascular canals (red) and diagenetic porosity (green) with respect to the total porosity are reported for each bone analysed (e.d.s. 10%); b) Distribution of volumes and c) cumulative frequency of the vascular canal pores. (For interpretation of the references to colour in this figure legend, the reader is referred to the Web version of this article.)

The total porosity of the juvenile bone is mainly influenced by the original bone, and the highest values are obtained from the sample of the Middle age. An increase of porosity during diagenesis is reported in the literature (Smith et al., 2008). However, this could not be confirmed in our study, as the percentage of diagenetic porosity decreases with the archaeological age. Hence, the prominent general re-organisation of the original microstructure in the cortical bone tissue in juvenile skeletons induces a rearrangement of the bone inorganic fraction into a denser fabric structure, leading to a decrease of porosity in the most ancient sample. Although bone porosity reflects variations of organic and inorganic components within the tissue (Nielsen-Marsh and Hedges, 2000; Smith et al., 2007; Turner-Walker et al., 2002), care is required in using it as a marker of the post-mortem bone deterioration in juvenile bones.

A comparison between the preservation degrees of the cortical bone

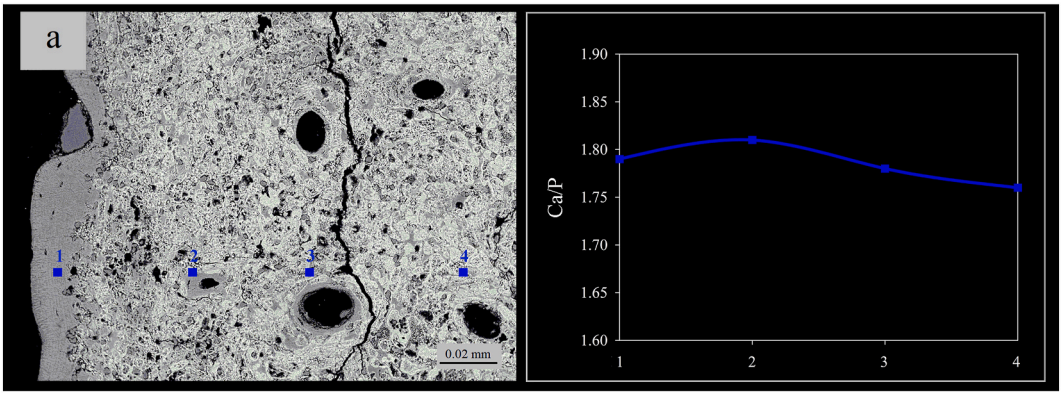

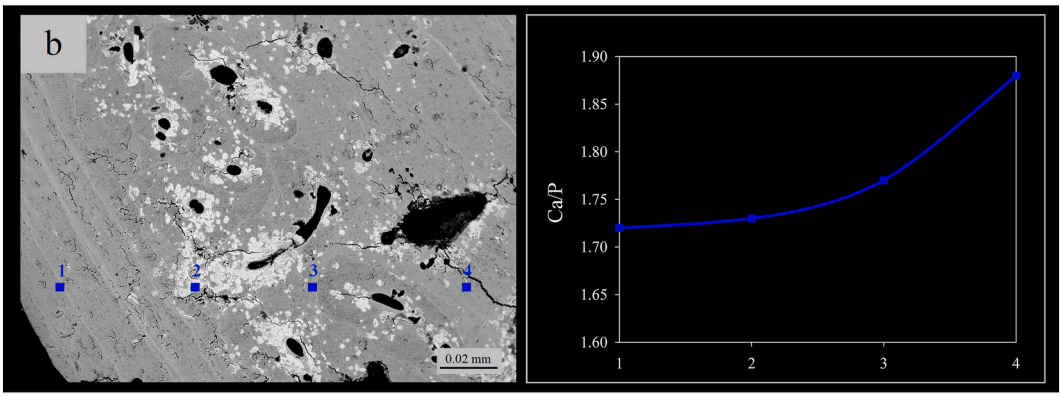

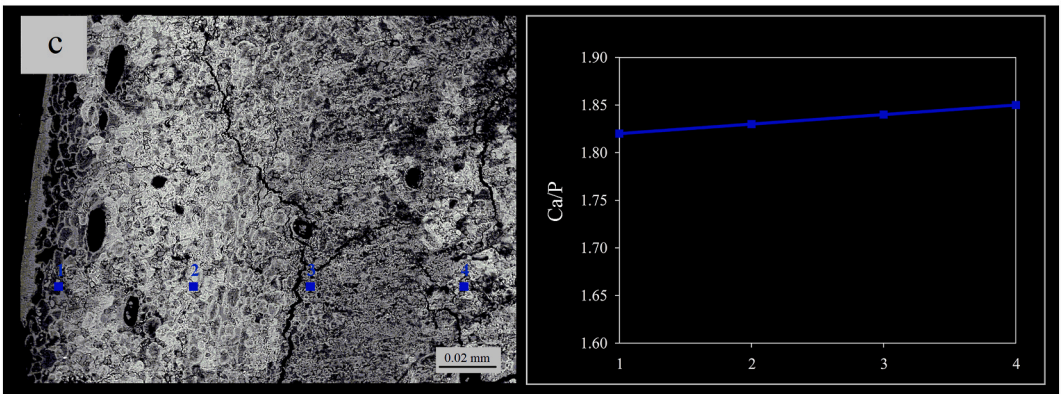

Bone zone	Gray scale value	Description
Unaltered zone	Highest grey scale value	Zone where the original bone microstructural features are well preserved and recognized
Re-mineralized zone	Bright-greyish grey scale value	Originates from the bone mineral re-deposition owing to the microbial activity
Altered zone	Lowest grey scale value	Characterized by large and irregular grooves, as well as small pores and thin channels, that appear as empty voids black in color, previously filled with colonies of microorganisms.

Fig. 4. Details of different preserved bones observed through BSE-SEM micrographs. For each bone, the results of chemical analysis, in term of Ca/P ratio, of four selected points, displayed from outer to inner bone edge, are provided in graphs a) UC_2, b) VM_1, c) VS_1, and d) PB_1. The figure reports a brief description of the different bone zones detected according to the greyscale values of the analysed samples.

tissue in archaeological adult human skeletons, as per Caruso et al. (2020), with that of juvenile bones shows analogies and differences. In juveniles, a lower degree of total porosity (5% vol) is observed, constituted by a small percentage of pores from diagenetic damages. On the contrary, in adult bones the percentage of total porosity reaches 12% vol and is mainly attributed to the diagenesis. This confirms the above-mentioned general re-organisation of the original bone microstructure in comparison with the mature tissue. On the contrary, a similarity between the two age groups is observed in the percentage of the vascular canal porosity.

In juvenile bones, vascular canal pores result in smaller volumes less than 10^{-6} mm^3. In contrast, largest pore volumes of adult bone range

Table 1
Electron microprobe analysis performed on thin sections of sample *UC_2, VM_1, VS_1* (wt%). Each result is calculated as an average of 30 points (e.d.s 10%).

	Late Roman age	Middle age	Modern age
	UC_2J	***VM_1J***	***VS_1J***
CaO	46.66	45.25	46.49
P_2O_5	33.23	30.5	32.33
Na_2O	0.31	0.41	0.36
SrO	0.06	0.06	0.06
MnO	0.01	0.01	0.01
MgO	0.30	1.22	0.36
SiO_2	0.07	0.03	0.12
SO_3	0.36	0.31	0.28
FeO	0.18	0.03	0.19
K_2O	0.02	0.04	0.02
Al_2O_3	0.13	0.02	0.04
BaO	0.03	0.02	0.02
Ce_2O_3	0.03	0.04	0.05
La_2O_3	0.04	0.01	0.03
Cl	0.02	0.04	0.03
Total	81.46	77.98	80.37
Ca/P	1.78	1.88	1.82

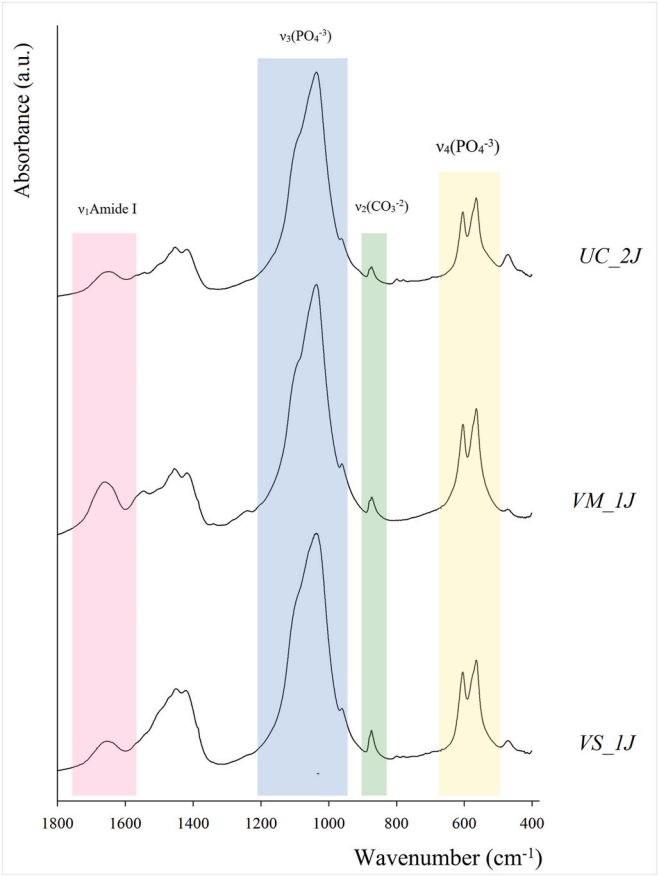

Fig. 5. Example of representative normalised Fourier transform infrared spectra collected from archaeological juvenile human bones and fresh immature pig bones.

between 10^{-5} mm^3 and 10^{-3} mm^3. The vascular canal sizes are highly degraded, but larger diameters are observed in adults in comparison with juveniles (0.025 and 0.14 and mm respectively). Finally, in archaeological adult bones, the vascular canal connectivity is better preserved than in juveniles, in which a full loss occurs.

Therefore, the rate of conservation of original porosity in children is

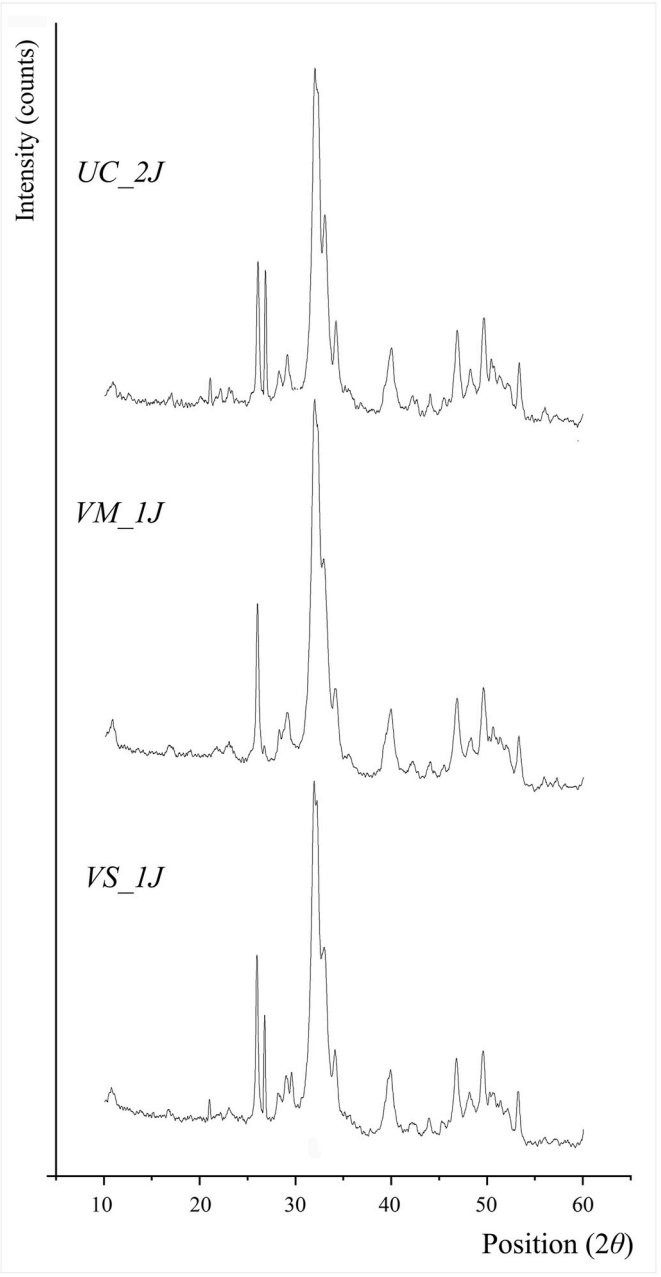

Fig. 6. Inset of the most representative peaks of hydroxyapatite carried out by X-ray powder diffraction measurements performed on juvenile human bones.

mainly affected by the stage of bone growth at death, rather than by diagenetic aspects; hormones, diet, metabolisms, biomechanics, and diseases significantly influence the 3D vascular pore microstructure (porosity and pore morphology) in lifetime (Bala et al., 2016). The high variation of histological preservation of analysed bones under the same burial setting (i.e. *VM_1J* vs. *VM_2J*) along with the large heterogeneous value of natural and diagenetic porosity observed in the present work, confirm that each bone tends to follow a particular degradation path, even in the same site-environmental context (Caruso et al., 2018, 2020; Jans et al., 2002; Nielsen-Marsh and Hedges, 2000; Rogoz et al., 2012; Smith et al., 2002; Trueman and Martin, 2002; Turner-Walker, 2012). Thus, the bone histology at death and the different type and scale of diagenetic alteration in the depositional environment might have a key role in bone degradation, especially for juvenile bones (Boaks et al., 2014; Collins et al., 2002; Eriksen et al., 2020; Kendall et al., 2018; Ross and Hale, 2018; Smith et al., 2007; White and Booth, 2014).

From a mineralogical point of view, hydroxyapatite appears as the main phase. Contents of quartz (10–30 wt%) are seen in specimens, mostly of the Late Roman period, because of the incorporation of burial soil (Margariti et al., 2019; Piga et al., 2013). No evidence of minor phases such as calcite, oxides, or sulphur are detected. Bioapatite commonly undergoes several re-crystallisation reactions to achieve a thermodynamically more stable structure configuration, characterised by a higher degree of crystal order, increased crystal size, and reduced specific surface area (Berna et al., 2004; Nielsen-Marsh and Hedges, 2000; Nielsen-Marsh et al., 2000). Our data indicate a linear correlation between the antiquity of specimens and the average micro-strain: A general decrease in micro-strain values and lattice defects with aging is observed, yielding a newly formed hydroxyapatite. The crystallographic refinement suggests that this process induces an increase of bioapatite unit cell volume, mainly due to an *a*-edge increase. This contradicts the reference data of fossil bones, where the unit cell volumes become smaller and closer to fluorapatite (Piga et al., 2013). These discrepancies might be explained by different ontogenetic growth stages of bone mineral crystallites at death: immature bones are generally constituted by a mixture of recently formed and mature crystallites (Dumont et al., 2011), thus influencing the diagenetic processes on mineral structures. On the contrary, similar average values are seen in terms of unit cell volumes (532 $Å^3$) for archaeological adult and juvenile bones.

Our micro-structure refinement highlights a nanometric size of the coherent diffraction domains, which exhibit a high heterogeneity of the average crystallite size along the crystallographic [001] direction, compared with reference data of fossil bones (Dumont et al., 2011; Piga et al., 2009, 2013). This indicates that the recrystallisation process is driven mostly by climatic and local burial conditions, which influenced the growth of bone minerals, thus inducing a preferred orientation, rather than by burial time.

Both in archaeological adult (Caruso et al., 2020) and juvenile human bones the coherent diffraction domains of bioapatite crystals are preferentially extended along the crystallographic *c*-axis. The indicative 3D model of the shape of the hydroxyapatite crystallites in juvenile bones preserves a platelet-like shape; an exception is the modern samples of the *VM* site, where a more needle-like shape is recorded (Dumont et al., 2011). On the contrary, in adults, a more spherical-like shape of the crystallites is observed in the Middle and Modern age specimens, and only the bones of the Late Roman age preserve a platelet-like shape that resembles the one recorded in contemporary bones.

The general reorganisation of the bone mineral phase during diagenesis also causes changes in the bone chemical composition. EMPA analyses on juvenile samples reveal that bioapatite crystals share chemical composition in terms of the average content of the major oxides. The average value of the Ca/P mole ratio observed here is lower than some figures from literature, reporting a ratio of 2.0–2.2 in bones of children aged 1–11 years, buried during 2500–2400 BCE (Szostek et al., 2011). The Ca/P mole ratio seems highly affected by local changes of the mineral fraction in bones, and a linear trend between the Ca/P and archaeological age in child remains cannot be established. Our results do not support the hypothesis that enrichment in calcium oxide occurs with the decaying of organic components and replacement of chemical elements in the original mineral lattice (Krajcarz, 2019 and references therein). Point analyses performed in three identified microstructure zones within each bone highlight discrepancies in terms of both major and minor oxides. In particular, the highest CaO contents are found in *re-mineralised zones,* due to the crystallisation of a new mineral phase (Berna et al., 2004; Margariti et al., 2019; Rogoz et al., 2012; Stathopoulou et al., 2008). In the other zones, minor elements substitute Ca or P sites in crystal sites of the original bioapatite. Sodium, silicon, aluminium, sulphur, and iron oxides are either mediated by physiological processes (Keenan et al., 2015; Margariti et al., 2019) or uptaken from the burial environment (i.e. groundwater and soil; Bayari et al., 2020; López-Costas et al., 2016; Rogoz et al., 2012), or derived from the decomposition process as well as from local microbial activity (Collins et al., 2002; Krajcarz, 2019).

The comparison between our results from juveniles and adult skeletons (Caruso et al., 2020) are consistent with the fact that the composition of the archaeological remains is highly site-sensitive and varies even within a single bone or between bones from the same site (Keenan, 2016 and references therein). Many studies have employed bone geochemistry to record the nature of soil where the skeletal remains originated (Krajcarz, 2019 and references therein). However, in this study, the low amount of minor oxides restricts a precise evaluation of the chemical alterations in respect of a particular type of burial sediment. Microbial activities may have also facilitated the relocation of some ions from the ground to bones. Microbial growth is promoted by moisture (Krajcarz, 2019 and references therein) and neutral pH conditions (Collins et al., 2002). Wetting–drying cycles may enhance trace elements' movement into the bone, even without biological activity (Krajcarz, 2019 and references therein).

FT-IR spectroscopy reports a clear relation between weathering of the bone mineral structure (depletion of carbonate ions, high crystallinity, and increase of crystal length) and time elapsed from death. In particular, (*i*) the higher the carbonate to phosphate ratio, the lower the bone age (Beasley et al., 2014; Hollund et al., 2013; Keenan et al., 2015; Lebon et al., 2011; Margariti et al., 2019; Reiche et al., 2010; Szostek et al., 2011 and references therein), thus confirming that as the diagenesis proceeds, the degradation of the organic phase promotes mineral changes, favouring the recrystallisation of the bone mineral fraction. Juvenile bones show a lower carbonate content in comparison with reference data of adult humans and animal fossil bones (Beasley et al., 2014; Caruso et al., 2020; Hollund et al., 2013; Keenan et al., 2015; Kontopoulos et al., 2019; Lebon et al., 2011; Margariti et al., 2019; Reiche et al., 2010; Szostek et al., 2011). Therefore, our data reflect a maturation process of bioapatite crystals, which involves enrichment of the carbonate content in the mineral lattice during the skeletal growth (Meneghini et al., 2003; Petra et al., 2005); (*ii*) the crystallinity index (IRSF) linearly increases with the sample antiquity, in agreement with reference values (Caruso et al., 2020; Hollund et al., 2013; Keenan et al., 2015; Margariti et al., 2019; Szostek et al., 2011; Thompson et al., 2009; Trueman et al., 2004); (*iii*) changes of mineral crystallinity are related to crystal sizes: a higher mean crystal length is observed in archaeological juvenile bones (~50–56 nm) when compared with the reference archaeological samples (Kontopoulos et al., 2019), in agreement with the Ostwald ripening mechanism (Arantes et al., 2018). FT-IR does not allow us to establish a positive correlation between the organic content and bone age, since collagen deterioration (swelling and hydrolysis) may depend on several factors (i.e. high temperature, acidic pH, and organic acids released by microbes; Collins et al., 2002; France et al., 2014; Hollund et al., 2013; Keenan et al., 2015; Lebon et al., 2011, 2016; Nielsen-Marsh and Hedges, 2000; Nielsen-Marsh et al., 2000; Reiche et al., 2010). Furthermore, the preservation of the collagen content does not correlate with the mineral dissolution, as expected (Collins et al., 2002). This can be ascribed to the modification of organo-mineral constituents in terms of organisation, quality, and quantity occurring in an immature tissue during growth and development. In the age range between 1.5 and 14 years, the bone tissue has a poorly organised matrix, characterised by a very porous microstructure, rich in collagen that tends to incorporate few minerals (Zimmermann et al., 2019). The contrary is expected in mature tissue (Beresheim et al., 2020). With growth, the bone turnover is significantly reduced, and the mineralisation of the tissue matrix increases (crystal size, perfection, and carbonation), improving the bone mechanical properties (Zimmermann et al., 2019).

A similar pattern of mineral alteration was observed in archaeological adult bones over time, considering the loss of organic carbonate and the increase of mineral crystallinity (Caruso et al., 2020). In juvenile bones, the amount of organic carbonate is further reduced and the mineral fraction results in a more crystalline phase (higher IRSF and mean crystal length). Adult skeletons exhibit a positive correlation

between the availability of organic content and samples' ages, at variance with children's bones. These different conservation degrees of bone constituents in mature and immature tissues within the same archaeological burial contexts may be explained by the different rates of bone turnover at death. In juveniles, the microstructure of the bone is variable since this changes considerably through growth and development (Pfeiffer, 2006).

6. Conclusions

This study uses a multidisciplinary approach – combining different conventional and unconventional techniques – to characterise the preservation state of a set of juvenile skeletal remains from different burial settings in Milan, Italy.

Different preservation rates are revealed between juvenile and adult bones, with a lesser fraction of undisturbed microstructure in juvenile remains. The organic fraction is highly variable in quality, quantity, and arrangement, even within a single bone. The 3D investigations confirm that the original bone microstructure is critically damaged. Furthermore, the morphometric results for the porous phase considerably differ from sample to sample – in terms of vascular canal volumes, interconnections, and diameters – even in samples sharing the same histological preservation. Discordant trends are observable for the shape, size, and orientation of bioapatite over the archaeological age. This is possibly related to the different ontogenetic growth stages of the bone mineral crystallites at death in children. The general reorganisation of the mineral fraction during diagenesis induces changes in the bone chemical composition, which appears highly site-sensitive and varies significantly even within a single bone or between bones from the same site.

In summary, our results from the combination of 2D and 3D imaging techniques, chemical and structural analyses, point to a high intra-individual skeletal preservation in archaeological juvenile bones, suggesting that immature and mature bone tissues deteriorate at different rates. This occurs primarily due to their intrinsic features (shape, porosity, histological structures, etc.), and secondarily, under the influence of the burial environment.

Authorship

V.C. and N.M. wrote the main manuscript text. V.C. and V.D. performed the EMP analysis and interpreted the results. V.C. and E.P. performed the FT-IR analysis and elaborated on the data. V.C. and N.M. performed XRPD and elaborated on the data. V.C. and C.C. elaborated on the OM data. V.C., N.M., and L.M. performed the SR-μCT analysis and elaborated the data. A.P. and F.B. revised the initial draft of the manuscript. All authors assisted in data interpretation and revision of the manuscript.

Ethics

Archaeological human bones were provided by the Laboratorio di Antropologia e Odontologia Forense (LABANOF) of Università degli Studi di Milano (Milan, Italy), in accordance with the Soprintendenza Archeologica Belle Arti e Paesaggio per la città metropolitana di Milano.

Declaration of competing interest

None.

Acknowledgements

The authors would like to thank all the staff of the SYRMEP (SYnchrotron Radiation for MEdical Physics) beamline at Elettra Sincrotrone Trieste (Basovizza, Italy) who assisted us during our data collection and the staff of the EMP and XRD laboratories of the Dipartimento di Scienze della Terra 'Ardito Desio', Università degli Studi di Milano (Milan, Italy) for their precious technical support with our data collection.

Appendix A. Supplementary data

Supplementary data to this article can be found online at https://doi.org/10.1016/j.jas.2021.105477.

Funding

This work was supported by the Fondazione Fratelli Confalonieri (Milan); and the project PRIN 2017-2017L83S77 (Italian Ministry for Education, University and Research, MIUR).

References

Arantes, T.M., Coimbra, L.M.M., Cristovan, F.H., Arantes, T.M., Rosa, G.M., Lião, L.M., 2018. Synthesis and optimization of colloidal hydroxyapatite nanoparticles by hydrothermal processes. J. Braz. Chem. Soc. 29, 1894–1903. https://doi.org/10.21577/0103-5053.20180065.

Bala, Y., Lefèvre, E., Roux, J.-P., Baron, C., Lasaygues, P., Pithioux, M., Kaftandjian, V., Follet, H., 2016. Pore network microarchitecture influences human cortical bone elasticity during growth and aging. J. Mech. Behav. Biomed. Mat. 63, 164–173. https://doi.org/10.1016/j.jmbbm.2016.05.018.

Barth, H.D., Zimmermann, E.A., Schaible, E., Tang, S.Y., Alliston, T., Ritchie, R.O., 2011. Characterization of the effects of X-ray irradiation on the hierarchical structure and mechanical properties of human cortical bone. Biomat 32, 8892–8904. https://doi.org/10.1016/j.biomaterials.2011.08.013.

Bayari, S.H., Özdemir, K., Sen, E.H., Araujo-Andrade, C., Erdal, Y.S., 2020. Application of ATR-FTIR spectroscopy and chemometrics for the discrimination of human bone remains from different archaeological sites in Turkey. Spectrochimi. Acta A: Mol. Biomol. Spectrosc. 237, 118311 https://doi.org/10.1016/j.saa.2020.118311.

Beasley, M.M., Bartelink, E.J., Taylor, L., Miller, R.M., 2014. Comparison of transmission FTIR, ATR, and DRIFT spectra: implications for assessment of bone bioapatite diagenesis. J. Archaeol. Sci. 46, 16–22. https://doi.org/10.1016/j.jas.2014.03.008.

Beresheim, A.C., Pfeiffer, S., Grynpas, M., 2020. Ontogenetic changes to bone microstructure in anarchaeologically derived sample of human ribs. J. Anat. 236, 448–462. https://doi.org/10.1111/joa.13116.

Berna, F., Matthews, A., Weiner, S., 2004. Solubilities of bone mineral from archaeological sites: the recrystallization window. J. Archaeol. Sci. 31, 867–882. https://doi.org/10.1016/j.jas.2003.12.003.

Boaks, A., Siwek, D., Mortazavi, F., 2014. The temporal degradation of bone collagen: a histochemical approach. Forensic Sci. Int. 240, 104–110. https://doi.org/10.1016/j.forsciint.2014.04.008.

Booth, T.J., 2016. An investigation into the relationship between funerary treatment and bacterial bioerosion in European archaeological human bone. Archaeometry 58, 484–499. https://doi.org/10.1111/arcm.12190.

Booth, T.J., Redfern, R.C., Gowland, R.L., 2016. Immaculate conceptions: micro-CT analysis of diagenesis in Romano-British infant skeletons. J. Archaeol. Sci. 74, 124–134. https://doi.org/10.1016/j.jas.2016.08.007.

Borić, D., Stefanović, S., 2004. Birth and death: infant burials from Vlasac and Lepenski Vir. Antiquity 78, 526–546. https://doi.org/10.1017/s0003598x00113201.

Bousson, V., Meunier, A., Bergot, C., Vicaut, É., Rocha, M.A., Morais, M.H., Laval-Jeantet, A.-M., Laredo, J.-D., 2001. Distribution of intracortical porosity in human midfemoral cortex by age and gender. J. Bone Miner. Res. 16, 1308–1317. https://doi.org/10.1359/jbmr.2001.16.7.1308.

Brun, F., Pacilè, S., Accardo, A., Kourousias, G., Dreossi, D., Mancini, L., Tromba, G., Pugliese, R., 2015. Enhanced and flexible software tools for X-ray computed tomography at the Italian synchrotron radiation facility Elettra. Fundam. Inf. 141, 233–243. https://doi.org/10.3233/fi-2015-1273.

Buckberry, J., 2000. Missing, presumed buried? Bone diagenesis and the under-representation of Anglo-Saxon children. In: Assemblage, vol. 5.

Caruso, V., Sguazza, E., Sassi, F., Gibelli, D., Ceresa Mori, A., Cattaneo, C., 2013. Gli scheletri della fossa comune di viale Sabotino a Milano: le vittime della peste manzoniana? Fasti Online. Folder-it-2013-285.

Caruso, V., Cummaudo, M., Maderna, E., Cappella, A., Caudullo, G., Scarpulla, V., Cattaneo, C., 2018. A comparative analysis of microscopic alterations in modern and ancient undecalcified and decalcified dry bones. Am. J. Phys. Anthropol. 165, 363–369. https://doi.org/10.1002/ajpa.23348.

Caruso, V., Marinoni, N., Diella, V., Berna, F., Cantaluppi, M., Mancini, L., Trombino, L., Cattaneo, C., Pastero, L., Pavese, A., 2020. Bone diagenesis in archaeological and contemporary human remains: an investigation of bone 3D microstructure and minero-chemical assessment. Archaeol. Anthropol. Sci. 12, 162 https://doi.org/10.1007/s12520-020-01090-6.

Cattaneo, C., Gibelli, D., Caruso, V., 2015. Antichi popoli di Valtellina. Analisi paleobiologiche sui resti scheletrici tra Tardi Antico, Medioevo e Rinascimento. In: Mariotti, V. (Ed.), La Valtellina nei secoli: studi e ricerche archeologiche. Vol II: ricerche e materiali archeologici, pp. 875–974.

Chacheva, M., 2015. Trinkets for the afterlife: personal ornaments from graves of children in the necropolis of Apollonia Pontica. Archaeologia Bulgarica 19 (1), 1–21.

Collins, M.J., Nielsen-Marsh, C.M., Hiller, J., Smith, C.I., Roberts, J.P., Prigodich, R.V., Wess, T.J., Csapò, J., Millard, A.R., Turner-Walker, G., 2002. The survival of organic matter in bone: a review. Archaeometry 44, 383–394. https://doi.org/10.1111/1475-4754.t01-1-00071.

Dal Sasso, G., Maritan, L., Usai, D., Angelini, I., Artioli, G., 2014. Bone diagenesis at the micro-scale: bone alteration patterns during multiple burial phases at Al Khiday (Khartoum, Sudan) between the Early Holocene and the II century AD. Palaeogeogr. Palaeoclimatol. Palaeoecol. 416, 30–42. https://doi.org/10.1016/j.palaeo.2014.06.034.

Dal Sasso, G., Lebon, M., Angelini, I., Maritan, L., Usai, D., Artioli, G., 2016. Bone diagenesis variability among multiple burial phases at Al Khiday (Sudan) investigated by ATR-FTIR spectroscopy. Palaeogeogr. Palaeoclimatol. Palaeoecol. 463, 168–179. https://doi.org/10.1016/j.palaeo.2016.10.005.

Djurić, M., Djukić, K., Milovanović, P., Janović, A., Milenković, P., 2011. Representing children in excavated cemeteries: the intrinsic preservation factor. Antiquity 85, 250–262. https://doi.org/10.1017/s0003598x00067582.

Dumont, M., Kostka, A., Sander, P.M., Borbely, A., Kaysser-Pyzalla, A., 2011. Size and size distribution of apatite crystals in sauropod fossil bones. Palaeogeogr. Palaeoclimatol. Palaeoecol. 310, 108–116. https://doi.org/10.1016/j.palaeo.2011.06.021.

Eriksen, A.M.H., Nielsen, T.K., Matthiesen, H., Carøe, C., Hansen, L.H., Gregory, D.J., Turner-Walker, G., Collins, M.J., Gilbert, M.T.P., 2020. Bone biodeterioration: the effect of marine and terrestrial depositional environments on early diagenesis and bone bacterial community. PloS One 15, e0240512. https://doi.org/10.1371/journal.pone.0240512.

France, C.A.M., Thomas, D.B., Doney, C.R., Madden, O., 2014. FT-Raman spectroscopy as a method for screening collagen diagenesis in bone. J. Archaeol. Sci. 42, 346–355. https://doi.org/10.1016/j.jas.2013.11.020.

Fratzl, P., Gupta, H.S., Paschalis, E.P., Roschger, P., 2004. Structure and mechanical quality of the collagen-mineral nano-composite in bone. J. Mater. Chem. 14, 2115–2123. https://doi.org/10.1039/b402005g.

Gardeła, L., Duma, P., 2013. Untimely death: atypical burials of children in Early and Late Medieval Poland. World Archaeol. 45, 314–332. https://doi.org/10.1080/00438243.2013.799040.

Georgiadis, M., 2011. Child burials in Mesolithic and Neolithic southern Greece: a synthesis. Child. Past 4, 31–45. https://doi.org/10.1179/cip.2011.4.1.31.

Goren, H.P., Agarwal, S.C., Beauchesne, P., 2020. Interpreting mortuary treatment from histological bone diagenesis: a case study from Neolithic Çatalhöyük. Int. J. Osteoarchaeol. 31, 121–134. https://doi.org/10.1002/oa.2930.

Groza, V.-M., Petraru, O.-M., Bejenaru, L., Popovici, M., 2020. Anthropological data on the 16th–19th century necropolis discovered at Aroneanu Monastery (Iaşi county, Romania). Memoirs of the Scientific Sections of the Romanian Academy Tome XLIII, 225–239.

Guy, H., Masset, C., Baud, C.-A., 1997. Infant taphonomy. Int. J. Osteoarchaeol. 7, 221–229. https://doi.org/10.1002/(sici)1099-1212(199705)7:3%3C221::aid-oa338%3E3.0.co;2-z.

Hedges, R.E.M., Millard, A.P., Pike, A.W.G., 1995. Measurements and relationships of diagenetic alteration of bone from three archaeological sites. J. Archaeol. Sci. 22, 201–209. https://doi.org/10.1006/jasc.1995.0022.

Hesse, B., Männicke, N., Pacureanu, A., Varga, P., Langer, M., Maurer, P., Peyrin, F., Raum, K., 2014. Accessing osteocyte lacunar geometrical properties in human jaw bone on the submicron length scale using synchrotron radiation μCT. J. Microsc. 255, 158–168. https://doi.org/10.1111/jmi.12147.

Hollund, H.I., Aariese, F., Fernandes, R., Jans, M.M.E., Kars, K., 2013. Testing an alternative high-throughput tool for investigating bone diagenesis: FTIR in attenuated total reflection (ATR) mode. Archaeometry 55, 507–532. https://doi.org/10.1111/j.1475-4754.2012.00695.x.

Jans, M.M.E., Kars, H., Nielsen-Marsh, C.M., Smith, C.I., Nord, A.G., Arthur, P., Earl, N., 2002. In situ preservation of archaeological bone: a histological study within a multidisciplinary approach. Archaeometry 44, 343–352. https://doi.org/10.1111/1475-4754.t01-1-00067.

Jans, M.M.E., Nielsen-Marsh, C.M., Smith, C.I., Collins, M.J., Kars, H., 2004. Characterization of microbial attack on archaeological bone. J. Archaeol. Sci. 31, 87–95. https://doi.org/10.1016/j.jas.2003.07.007.

Kay, J.E., 2016. Children's burials in fifth-century Britain and connections to the Roman past. Child. Past 9, 86–108. https://doi.org/10.1080/17585716.2016.1205340.

Keenan, S.W., 2016. From bone to fossil: a review of the diagenesis of bioapatite. Am. Mineral. 101, 1943–1951. https://doi.org/10.2138/am-2016-5737.

Keenan, S.W., Engel, A.S., 2017. Early diagenesis and recrystallization of bone. Geochem. Cosmochim. Acta 196, 209–223. https://doi.org/10.1016/j.gca.2016.09.033.

Keenan, S.W., Engel, A.S., Roy, A., Bovenkamp-Langlois, G.L., 2015. Evaluating the consequences of diagenesis and fossilization on bioapatite lattice structure and composition. Chem. Geol. 413, 18–27. https://doi.org/10.1016/j.chemgeo.2015.08.005.

Kendall, C., Eriksen, A.M.H., Kontopoulos, I., Collins, M.J., Turner-Walker, G., 2018. Diagenesis of archaeological bone and tooth. Palaeogeogr. Palaeoclimatol. Palaeoecol. 491, 21–37. https://doi.org/10.1016/j.palaeo.2017.11.041.

Kontopoulos, I., Nystrom, P., White, L., 2016. Experimental taphonomy: post-mortem microstructural modifications in Sus scrofa domesticus bone. Forensic Sci. Int. 266, 320–328. https://doi.org/10.1016/j.forsciint.2016.06.024.

Kontopoulos, I., Penkman, K., Liritzis, I., Collins, M.J., 2019. Bone diagenesis in a Mycenaean secondary burial (Kastrouli, Greece). Archaeol. Anthropol. Sci. 11, 5213–5230. https://doi.org/10.1007/s12520-019-00853-0.

Krajcarz, M.T., 2019. Alteration of the metal content in animal bones after 2.5-year experimental exposure to sediments. Archaeol. Anthropol. Sci. 11, 361–372. https://doi.org/10.1007/s12520-017-0533-2.

Lebon, M., Müller, K., Bahain, J., Fröhlich, F., Falguères, C., Bertrand, L., Sandt, C., Reiche, I., 2011. Imaging fossil bone alterations at the microscale by SR-FTIR microspectroscopy. J. Anal. At. Spectrom. 26, 922–929. https://doi.org/10.1039/C0JA00250J.

Lebon, M., Reiche, I., Gallet, X., Bellot-Gurlet, L., Zazzo, A., 2016. Rapid quantification of bone collagen content by ATR-FTIR spectroscopy. Radiocarbon 58, 131–145. https://doi.org/10.1017/RDC.2015.11.

Lewis, M.E., 2007. The Bioarchaeology of Children: Perspectives from Biological and Forensic Anthropology. Cambridge University Press, Cambridge.

López-Costas, O., Lantes-Suárez, O., Martínez Cortizas, A., 2016. Chemical compositional changes in archaeological human bones due to diagenesis: type of bone vs soil environment. J. Archaeol. Sci. 67, 43–51. https://doi.org/10.1016/j.jas.2016.02.001.

Manifold, B.M., 2010. The representation of non-adult skeletal elements recovered from British archaeological sites. Child. Past 3, 43–62. https://doi.org/10.1179/cip.2010.3.1.43.

Manifold, B.M., 2012. Intrinsic and extrinsic factors involved in the preservation of non-adult skeletal remains in archaeology and forensic science. Bull. Int. Assoc. Paleodontol. 6, 51–69.

Manifold, B.M., 2013. Differential preservation of children's bones and teeth recovered from early medieval cemeteries: possible influence for the forensic recovery of non-adult skeletal remains. Anthropol. Rev. 76, 23–49. https://doi.org/10.2478/anre-2013-0007.

Manifold, B.M., 2014. Bone mineral density in children from anthropological and clinical science: a review. Anthropol. Rev. 77, 111–135. https://doi.org/10.2478/anre-2014-0011.

Margariti, E., Stathopoulou, E.T., Sanakis, Y., Kotopoulou, E., Pavlakis, P., Godelitsas, A., 2019. A geochemical approach to fossilization processes in Miocene vertebrate bones from Sahabi, NE Libya. J. Afr. Earth Sci. 149, 1–18. https://doi.org/10.1016/j.jafrearsci.2018.07.019.

Meneghini, C., Dalconi, M.C., Nuzzo, S., Mobilio, S., Wenk, R.H., 2003. Rietveld refinement on X-ray diffraction patterns of bioapatite in human fetal bones. Biophys. J. 84, 2021–2029. https://doi.org/10.1016/s0006-3495(03)75010-3.

Nava, A., Coppa, A., Coppola, D., Mancini, L., Dreossi, D., Zanini, F., Bernardini, F., Tuniz, C., Bondioli, L., 2017. Virtual histological assessment of the prenatal life history and age at death of the Upper Paleolithic fetus from Ostuni (Italy). Sci. Rep. 7, 9427 https://doi.org/10.1038/s41598-017-09773-2.

Nielsen-Marsh, C.M., Hedges, R.E.M., 2000. Patterns of diagenesis in bone I: the effects of site environments. J. Archaeol. Sci. 27, 1139–1150. https://doi.org/10.1006/jasc.1999.0537.

Nielsen-Marsh, C., Gernaey, A., Turner-Walker, G., Hedges, R., Pike, A.W.G., Collins, M., 2000. The chemical degradation of bone. In: Cox, M., Mays, S. (Eds.), Human Osteology: in Archaeology and Forensic Science. Cambridge University Press, Cambridge, pp. 439–454.

Paganin, D., Mayo, S.C., Gureyev, T.E., Miller, P.R., Wilkins, S.W., 2002. Simultaneous phase and amplitude extraction from a single defocused image of a homogeneous object. J. Microsc. 206, 33–40. https://doi.org/10.1046/j.1365-2818.2002.01010.x.

Pacureanu, A., Langer, M., Boller, E., Tafforeau, P., Peyrin, F., 2012. Nanoscale imaging of the bone cell network with synchrotron X-ray tomography: optimization of acquisition setup. Med. Phys. 39, 2229–2238.

Petra, M., Anastassopoulou, J., Theologis, T., Theophanides, T., 2005. Synchrotron micro-FT-IR spectroscopic evaluation of normal paediatric human bone. J. Mol. Struct. 733, 101–110. https://doi.org/10.1016/j.molstruc.2004.07.041.

Pfeiffer, S., 2006. Cortical bone histology in juveniles. In: Grupe, G., Peters, J. (Eds.), Bioarchaeological Remains under the Microscope, Documenta Archaeobiologiae, vol. 4. Verlag Maria Leidorf, Rahden, pp. 15–28.

Piga, G., Santos-Cubedo, A., Solà, S.M., Brunetti, A., Malgosa, A., Enzo, S., 2009. An X-ray diffraction (XRD) and X-ray fluorescence (XRF) investigation in human and animal fossil bones from Holocene to Middle Triassic. J. Archaeol. Sci. 36, 1857–1868. https://doi.org/10.1016/j.jas.2009.04.013.

Piga, G., Solinas, G., Thompson, T.J.U., Brunetti, A., Malgosa, A., Enzo, S., 2013. Is X-ray diffraction able to distinguish between animal and human bones? J. Archaeol. Sci. 40, 778–785. https://doi.org/10.1016/j.jas.2012.07.004.

Pitfield, R., Deter, C., Mahoney, P., 2019. Bone histomorphometric measures of physical activity in children from medieval England. Am. J. Phys. Anthropol. 169, 730–746. https://doi.org/10.1002/ajpa.23853.

Reiche, I., Lebon, M., Chadefaux, C., Müller, K., Le Hô, A.-S., Gensch, M., Schade, U., 2010. Microscale imaging of the preservation state of 5,000-year-old archaeological bones by synchrotron infrared microspectroscopy. Anal. Bioanal. Chem. 397, 2491–2499. https://doi.org/10.1007/s00216-010-3795-4.

Rivers, M., 1998. Tutorial Introduction to X-Ray Computed Microtomography Data Processing. http://wwwfp.mcs.anl.gov/xray-cmt/rivers/tutorial.html. (Accessed 28 August 2021).

Rogoz, A., Sawlowicz, Z., Wojtal, P., 2012. Diagenetic history of woolly mammoth (*Mammuthus primigenius*) skeletal remains from the archaeological site Cracow Spadzista street (B), Southern Poland. Palaios 27, 541–549.

Ross, A.H., Hale, A.R., 2018. Decomposition of juvenile-sized remains: a macro- and microscopic perspective. Forensic Sci. Res. 3, 310–319. https://doi.org/10.1080/20961790.2018.1489362.

Sanchez, S., Ahlberg, P.E., Trinajstic, K.M., Mirone, A., Tafforeau, P., 2012. Three-dimensional synchrotron virtual paleohistology: a new insight into the world of fossil bone microstructures. Microsc. Microanal. 18, 1095–1105. https://doi.org/10.1017/S1431927612001079.

Scheuer, L., Black, S., 2000. Developmental Juvenile Osteology. Academic Press, London.

Schnitzler, C.M., Mesquita, J.M., 2013. Cortical porosity in children is determined by age-dependent osteonal morphology. Bone 55, 476–486. https://doi.org/10.1016/j.bone.2013.03.021.

Smith, C.I., Nielsen-Marsh, C.M., Jans, M.M.E., Arthur, P., Nord, A.G., Collins, M.J., 2002. The strange case of Apigliano: early 'fossilization' of medieval bone in southern Italy. Archaeometry 44, 405–415.

Smith, C.I., Nielsen-Marsh, C.M., Jans, M.M.E., Collins, M.J., 2007. Bone diagenesis in the European Holocene I: patterns and mechanisms. J. Archaeol. Sci. 34, 1485–1493. https://doi.org/10.1016/j.jas.2006.11.006.

Smith, C.I., Faraldos, M., Fernández-Jalvo, Y., 2008. The precision of porosity measurements: effects of sample pre-treatment on porosity measurements of modern and archaeological bone. Palaeogeogr. Palaeoclimatol. Palaeoecol. 266, 175–182. https://doi.org/10.1016/j.palaeo.2008.03.028.

Smith, T.M., Tafforeau, P., Reid, D.J., Pouech, J., Lazzari, V., Zermeno, J.P., Guatelli-Steinberg, D., Olejniczak, A.J., Hoffman, A., Radovčić, J., Makaremi, M., Toussaint, M., Stringer, C., Hublin, J.-J., 2010. Dental evidence for ontogenetic differences between modern humans and Neanderthals. Proc. Natl. Acad. Sci. U.S.A. 107, 20923–20928. https://doi.org/10.1073/pnas.1010906107.

Stathopoulou, E.T., Psycharis, V., Chryssikos, G.D., Gionis, V., Theodorou, G., 2008. Bone diagenesis: new data from infrared spectroscopy and X-ray diffraction. Palaeogeogr. Palaeoclimatol. Palaeoecol. 266, 168–174. https://doi.org/10.1016/j.palaeo.2008.03.022.

Stroszeck, J., 2012. Grave gifts in child burials in the Athenian Kerameikos: the evidence of sea shells. In: Hermary, A., Dubois, C. (Eds.), L'enfant et la mort dans l'antiquité III : Le Matériel associé aux tombes d'enfants. Centre Camille Jullian, pp. 57–73.

Szostek, K., Stepańczak, B., Szczepanek, A., Kępa, M., Głąb, H., Jarosz, P., Włodarczak, P., Tunia, K., Pawlyta, J., Paluszkiewicz, C., Tylko, G., 2011. Diagenetic signals from ancient human remains: bioarchaeological applications. Mineralogia 42, 93–112. https://doi.org/10.2478/v10002-011-0009-4.

Thompson, T.J.U., Gauthier, M., Islam, M., 2009. The application of a new method of Fourier transform spectroscopy to the analysis of burned bone. J. Archaeol. Sci. 36, 910–914. https://doi.org/10.1016/j.jas.2008.11.013.

Trueman, C.N., Martin, D.M., 2002. The long-term survival of bone: the role of bioerosion. Archaeometry 44, 371–382. https://doi.org/10.1111/1475-4754.t01-1-00070.

Trueman, C.N.G., Behrensmeyer, A.K., Tuross, N., Weiner, S., 2004. Mineralogical and compositional changes in bones exposed on soil surfaces in Amboseli National Park, Kenya: diagenetic mechanisms and the role of sediment pore fluids. J. Archaeol. Sci. 31, 721–739. https://doi.org/10.1016/j.jas.2003.11.003.

Trueman, C.N., Privat, K., Field, J., 2008. Why do crystallinity values fail to predict the extent of diagenetic alteration of bone mineral? Palaeogeogr. Palaeoclimatol. Palaeoecol. 266, 160–167. https://doi.org/10.1016/j.palaeo.2008.03.038.

Turner-Walker, G., 2012. Early bioerosion in skeletal tissues: persistence through deep time. Neues Jahrb. Geol. Paläontol. 265, 165–183. https://doi.org/10.1127/0077-7749/2012/0253.

Turner-Walker, G., 2019. Light at the end of the tunnels? The origins of microbial bioerosion in mineralised collagen. Palaeogeogr. Palaeoclimatol. Palaeoecol. 529, 24–38. https://doi.org/10.1016/j.palaeo.2019.05.020.

Turner-Walker, G., Syversen, U., 2002. Quantifying histological changes in archaeological bones using BSE-SEM image analysis. Archaeometry 44, 461–468. https://doi.org/10.1111/1475-4754.t01-1-00078.

Turner-Walker, G., Nielsen-Marsh, C.M., Syversen, U., Kars, H., Collins, M.J., 2002. Sub-micron spongiform porosity is the major ultra-structural alteration occurring in archaeological bone. Int. J. Osteoarchaeol. 12, 407–414. https://doi.org/10.1002/oa.642.

Ubelaker, D.H., 1978. Human Skeletal Remains: Excavation, Analysis and Interpretation. Smithsonian Institute Press, Washington DC.

Van Aarle, W., Palenstijn, W.J., De Beenhouwer, J., Altantzis, T., Bals, S., Batenburg, K. J., Sijbers, J., 2015. The ASTRA Toolbox: a platform for advanced algorithm development in electron tomography. Ultramicroscopy 157, 35–47. https://doi.org/10.1016/j.ultramic.2015.05.002.

Weiner, S., Wagner, H.D., 1998. The material bone: structure-mechanical function relations. Annu. Rev. Mater. Sci. 28, 271–298. https://doi.org/10.1146/annurev.matsci.28.1.271.

White, L., Booth, T.J., 2014. The origin of bacteria responsible for bioerosion to the internal bone microstructure: results from experimentally-deposited pig carcasses. Forensic Sci. Int. 239, 92–102. https://doi.org/10.1016/j.forsciint.2014.03.024.

Wopenka, B., Pasteris, J.D., 2005. A mineralogical perspective on the apatite in bone. Mater. Sci. Eng. C 25, 131–143. https://doi.org/10.1016/j.msec.2005.01.008.

Young, R.A., 1993. The Rietveld Method. Oxford University Press, Oxford.

Zimmermann, E.A., Riedel, C., Schmidt, F.N., Stockhausen, K.E., Chushkin, Y., Schaible, E., Gludovatz, B., Vettorazzi, E., Zontone, F., Puschel, K., Amling, M., Ritchie, R.O., Busse, B., 2019. Mechanical competence and bone quality develop during skeletal growth. J. Bone Miner. Res. 34, 1461–1472. https://doi.org/10.1002/jbmr.3730.

Ērkšķe, A., 2020. The children are missing! Some thoughts on the underrepresentation of non-adult burials in Latvian Iron age cemeteries. Est. J. Archaeol. 24, 161–189. https://doi.org/10.3176/arch.2020.2.03.